Importance of Context in Protein Folding: Secondary Structural Propensities versus Tertiary Contact-Assisted Secondary Structure Formation†

Kathryn A. Scott, Darwin O. V. Alonso, Yongping Pan,‡ and Valerie Daggett*

Department of Medicinal Chemistry, University of Washington, Seattle, Washington 98195-7610

Received August 27, 2005; Revised Manuscript Received January 26, 2006

ABSTRACT: Molecular dynamics simulations can be used to reveal the detailed conformational behaviors of peptides and proteins. By comparing fragment and full-length protein simulations, we can investigate the role of each peptide segment in the folding process. Here, we take advantage of information regarding the helix formation process from our previous simulations of barnase and protein A as well as new simulations of four helical fragments from these proteins at three different temperatures, starting with both helical and extended structures. Segments with high helical propensity began the folding process by tethering the chain through side chain interactions involving either polar interactions, such as salt bridges, or hydrophobic staples. These tethers were frequently nonnative (i.e., not $i \rightarrow i + 4$ spacing) and provided a scaffold for other residues, thereby limiting the conformational search. The helical structure then propagated on both sides of the tether. Segments with low stability and propensity formed later in the folding process and utilized contacts with other portions of the protein when folding. These helices formed via a tertiary contact-assisted mechanism, primarily via hydrophobic contacts between residues distant in sequence. Thus, segments with different helical propensities appear to play different roles during protein folding. Furthermore, the active role of nonlocal side chains in helix formation highlights why we must move beyond simple hierarchical models of protein folding.

Numerous efforts have focused on the characterization of protein folding pathways (*1*−*7*). On the basis of experimental and simulation studies, two extreme models for protein folding have been considered historically: the framework (*8*−*11*) and hydrophobic collapse (*12*−*14*) models. Both models posit the existence of an intermediate(s) along the pathway and fail to explain the two-state folding mechanism of several small proteins. More recently, the nucleation−condensation mechanism was introduced to address this shortcoming (*15*). In this case, the formation of secondary and tertiary structures is coupled and concerted, coming together in the transition state. Patches on α-helices and hydrophobic residues distant in sequence typically serve as the nucleation sites (*16*). Once these come together, the collapse and condensation of the structure is relatively facile. In addition to explaining two-state folding behavior, the nucleation−condensation model can also describe three-state folding, and, in fact, it can be considered a combination of the two extreme models (*5*). Nucleation−condensation is something of a compromise between these two mechanisms, and we have recently shown how increases in the helical propensity cause a shift or slide from nucleation−condensation to the framework mechanism (*17*). In any case, to determine which folding model is operative, it is important to understand the role of secondary structure in folding, its formation, and the extent to which it is formed along the folding pathway for individual segments of a protein.

Here, we are interested in the mechanisms by which helices form. There is a large body of information about the folding of α-helical peptides, in particular, alanine-based peptides. Experimentally, ultrafast kinetic methods using temperature jump with IR, Raman, or fluorescence spectroscopy as a probe are necessary to study the folding and unfolding of helices. Depending on temperature and peptide composition, one or two phases may be seen in both folding and unfolding (*18*−*21*). In 1997, Eaton and co-workers made a direct observation of the rate of helix propagation, showing that propagation could occur on the 10's of ns time scale (*18*). Gai and co-workers studied alanine-based peptides from ∼20−40 residues in length with different *N*-caps or *N*-terminal capping sequences (*20*, *21*). In their work, they saw two phases in the kinetic trace. The slower of these, with a relaxation time typically on the 100's of ns time scale, was attributed to the helix−coil transition. The faster phase, occurring in less than the 10 ns rise time of their instrument, may arise from helix propagation (*20*). Their work showed that relaxation rates for peptides with good *N*-cap sequences are more rapid than those with poor *N*-cap sequences. They also demonstrated that the change in the helix folding rate with peptide length is nonlinear.

Molecular dynamics (MD)[1] studies can also give insight into the mechanism of helix−coil transitions as well as

† Financial support was provided by the National Institutes of Health (GM 50789).

* To whom correspondence should be addressed. E-mail: daggett@u.washington.edu.

‡ Current address: National Cancer Institute at Frederick, Frederick, MD 21702-1201.

[1] Abbreviations: α1, barnase helix 1; β(3−4), barnase beta strands 3 and 4; H1, protein A helix 1; H2, protein A helix 2; H3, protein A helix 3; MD, molecular dynamics.

10.1021/bi0517281 CCC: $33.50
Published on Web 03/08/2006

modeling equilibrium and kinetic properties (*22*). A number of groups have used implicit solvent models, with either a distance-dependent dielectric or a generalized Born continuum solvent for such simulations to improve sampling (*23*, *24*). Simulations of $(AAQAA)_3$ by Caflisch and co-workers show helix formation to be a non-two-state process with the possibility of multiple folding pathways, consistent with a conformational diffusional search process (*24*). In contrast, an alanine and lysine containing peptide studied by Duan and co-workers showed three kinetic phases related to nucleation, helix propagation, and breaking of side-chain hydrophobic contacts (*23*). Other recent studies have been carried out with explicit solvation (*25*−*29*). The Garcia group has used replica exchange MD to study a variety of peptides. In simulations of $(AAARA)_3A$, they showed that arginine sides chains shield backbone carbonyls and that these shielded carbonyl groups show a higher probability of helix formation (*25*). Their work also suggests that an explicit solvent may be necessary to accurately model helix formation by simulation and to get good agreement with experimental helix−coil parameters (*26*). Pande and co-workers recently investigated the folding of two 21-residue alanine-rich peptides (*29*). In these simulations, they saw multiple nucleation steps forming short helical segments from which the structure propagated to give the folded helix. A majority of studies on helical peptides are carried out on relatively small alanine-based peptides, with typically greater than 50% helical propensity. This poses two questions. Does the folding mechanism of a sequence with high helical propensity change when the sequence is part of a protein? Do sequences with low helical propensity that form helices in the native state fold in the same manner as those with high helical propensity?

Experiments can provide information about the extent of helix formation in intermediate states, transition states, and denatured states. However, they do not usually delineate precisely where the helical structure resides or give the details of the structural transitions between these discrete states. Such information can be obtained via MD simulations. MD simulations have provided reasonable models for the transition, intermediate, and even the denatured states of several proteins (*16*). One particularly unexpected finding was made many years ago in unfolding simulations of barnase (*30*, *31*) and protein A (*32*). Helix reformation was observed from partially and fully unfolded conformations. Analysis of these events should then provide direct details of the helix formation process. When combined and compared with simulations of the corresponding helical peptide fragments, we should be able to decipher the roles of inherent secondary structural propensity and both local and nonlocal interactions in helix formation. Furthermore, information about the kinetic stability of different helices and their structural propensities under different conditions as both fragments and full-length proteins should aid in the determination of the role of each individual helical segment in the folding process. To this end, we have performed such simulations of barnase and protein A and their respective helical fragments. In the case of barnase, previous simulations revealed a mechanism of contact-assisted helix formation for α1, that is, it only refolded after making contacts with another portion of the protein.

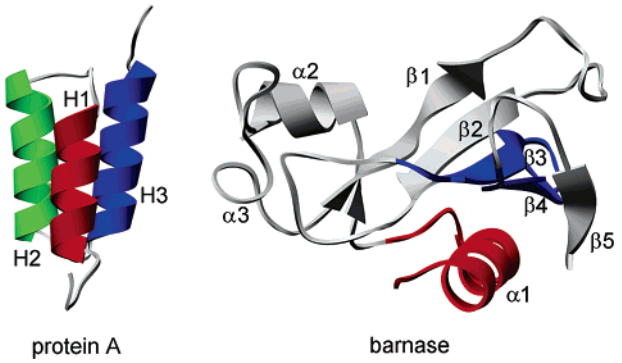

FIGURE 1: NMR solution structures of protein A E-domain (*56*) and barnase (*57*). The α1/β(3−4) region of barnase used in the fragment simulations is colored red and blue.

Barnase is a 110-residue, α+β ribonuclease (Figure 1). The folding of barnase has been particularly well described through both experiments (*31*, *33*−*38*) and simulations from different groups (*30*, *31*, *39*−*44*). In contrast, protein A is a membrane-bound protein from *Staphylococcus aureus* with five domains that bind to the Fc fragment of immunoglobulin G (*45*, *46*). The domains are homologous but not identical, and each domain is composed of three helices, which we denote as H1, H2, and H3 (Figure 1).

Protein A has been extensively studied by computational groups; work in this area was recently summarized in a commentary by Wolynes (*47*). Briefly, two different views of its folding behavior have been proposed. Several groups have proposed that H3 is the most stable and persistent helix on the basis of a range of methods including replica exchange MD, high-temperature unfolding simulations, and the solution of the stochastic difference equation (*32*, *48*, *49*). This result is in agreement with previous experimental work showing that the H3 peptide is the most stable in isolation with an approximately 50% helical population (*50*, *51*). Alternatively, work based on pathways along a pseudo free-energy surface constructed from short molecular dynamics trajectories predicts that H1 is the most stable helix and that it forms first during folding, leading to a stable intermediate (*52*, *53*). Theoretical studies of low-resolution protein models by Karplus and co-workers (*54*) might be consistent with either or both scenarios. The transition state for the folding of the B domain of protein A was recently characterized by Fersht and co-workers (*55*). Φ-values from alanine to glycine, scanning mutations at solvent-exposed positions, indicate that H2 is highly structured in the transition state, with H3 having some structure near the *N*-terminus and H1 being poorly structured.

To better understand helix formation in these two systems and the relative importance of helical propensity and tertiary contacts, we have performed multiple MD simulations of the helical fragments from these two proteins at different temperatures with different starting conformations as well as simulations of the full-length proteins. A majority of the studies on helix formation in simulation have focused on model alanine-based peptides, which are of limited utility in describing the much more complicated situations for real peptide and protein sequences. Our simulations suggest that helix formation in the fragments depends on the secondary structural propensities of the fragments, which in turn are determined by intrahelical side chain interactions as opposed

to true, inherent (ϕ,ψ) propensities. Segments with low propensities utilize contact with other parts of the protein to fold. On the basis of a comparison of fragment and full-length protein simulations, it appears that the formation of helical structure in portions of the sequence with high helical propensity occurs early in folding, and the remaining helices fold via a tertiary contact-assisted mechanism.

METHODS

Simulations were performed of helical and extended fragments from the E-domain of protein A and barnase. The helical fragments were excised from the NMR structure of the E-domain of protein A (*56*) and the crystal and NMR structures of barnase (*31*, *57*). The extended peptides were built with (ϕ,φ) angles of 180°.

All simulations were performed using an in-house version of the program ENCAD and a previously described force field (*58*, *59*). All protein and water atoms were explicitly represented. The fragments were minimized for 1000 steps in vacuo. The peptides were then solvated in a rectangular box with water extending at least 10−12 Å from any protein atom. The density of each box was set to the experimental value for the temperature of interest (0.939, 0.890, and 0.829 g/mL^3 at 398, 448, and 498 K, respectively (*60*, *61*)) by adjusting the box volume. At high temperatures, the protein (or peptide) traverses energy barriers. Although complete refolding is unfavorable under these conditions, some partially folded conformations should be sampled transiently. After setting the density, the box volume remained constant, using the NVE microcanonical ensemble. Periodic boundary conditions were employed to minimize edge effects. The systems were further equilibrated for 2000 steps of minimization of water, 2000 steps of molecular dynamics of water, 1000 steps of minimization of water, 500 steps of minimization of the peptide, and finally, 500 steps of minimization of the entire system. In the production simulations, an 8 Å force-shifted nonbonded cutoff was employed with the pair list was updated every five steps. A time step of 2 fs was used. The simulations were carried out for 10−25 ns, with most simulations running for 25 ns. Structures were saved every 0.2 ps for analysis.

Our earlier full-length protein A E domain simulation (referred to as E2 in our previous publication) was continued from 6−25 ns following the published protocols (*32*). The full-length and fragment simulations of barnase beginning from the native structure were performed earlier (*30*, *31*). The α1 fragment simulation beginning in an extended conformation is new to this study, and the protocol described above for protein A fragments was used. Molecular graphics images were produced using the UCSF Chimera package from the Resource for Biocomputing, Visualization, and Informatics at the University of California, San Francisco (supported by NIH P41 RR-01081) (*62*).

RESULTS

Previously, we observed a novel mode of helix formation in both barnase and protein A involving long-range tertiary contact-assisted catalysis (*30*−*32*). We begin here by briefly describing those results and note that all refolding steps described below are observed directly in the simulation; they are not inferred from unfolding. Then, we proceed with new results from the continuation of an earlier protein A simulation. We further investigate the importance of this mechanism of helix formation by performing numerous simulations of fragments corresponding to these helices. Specifically, we have carried out simulations of three fragments from the E domain of protein A and the α1 fragment of barnase, all at three different temperatures starting from both folded (helical) and extended structures. The sequences for each of the fragments are as follows:

Protein A H1: Ace-QQNAFYQVLQM-Nme, nine residues in helix

H2: Ace-NADQRNGFIQSLKD-Nme, 12 residues in helix

H3: Ace-QSANVLGEAQKLNDSQ-Nme, 14 residues in helix

Barnase α1: Ace-TFDGVADYLQTYHK−Nme, 12 residues in helix

The *N*-termini were acetylated (Ace) and the *C*-termini were capped with an *N*-methyl group (Nme). Some general features of these fragments are listed in Table 1.

Table 1: Residue-Based Properties of Each Peptide Fragment

fragment	# of residues	# of side -chain heavy atoms/res	% hydrophobic residues in sequence	# of C_β-branched residues	$i \rightarrow i+4$ spacing of side chains
protA-H1	9	4.5	56	1	favorable
protA-H2	12	4.0	33	1	favorable
protA-H3	14	3.5	36	1	favorable
barnase α1	12	4.2	55	2	favorable

Full-Length Barnase Simulations.

We first observed contact-assisted helix formation in the denatured state of barnase, that is, after it had unfolded (*30*, *31*). In all simulations, the α1 region was very dynamic in the denatured state. Residues 11−14 populated helical conformations much of the time, whereas residues 7−10 switched back and forth between helical and other conformational states. When Trp 94 together with other hydrophobic residues shifted to the center of α1, favorable hydrophobic interactions led to the readjustment of the conformations of the α1 residues, which induced helix formation.

This reorientation is illustrated in snapshots from a simulation beginning from the NMR structure (referred to as the D-1 simulation in our previous publications). Two nanoseconds into the simulation, α1 was partially unfolded with residues 7−12 having lost their helical conformations. However, most of the native hydrogen-bonding network was regained with time (Figure 2A). Between 2 and 2.5 ns, some contacts between α1 and β(3−4) were made, but the orientation of Ala 10 prevented helix formation at the *N*-terminus. After this time point, reorientation of the side chain contacts at the α1 and β(3−4) facilitated the folding of α1. The packing of hydrophobic residues between α1 and residues 88−89 increased as residues 7−12 were added to the helix (*30*). This packing decreased the combined solvent accessible hydrophobic surface area of Val 10, Ala 11, and Leu 14. The *C*-terminal end of the helix (residues 14−17) maintained a helical turn throughout the ensemble as judged by both backbone orientation and hydrogen bonding (*31*).

This contact-assisted helix formation and solvent exclusion were also observed in another independent denaturation

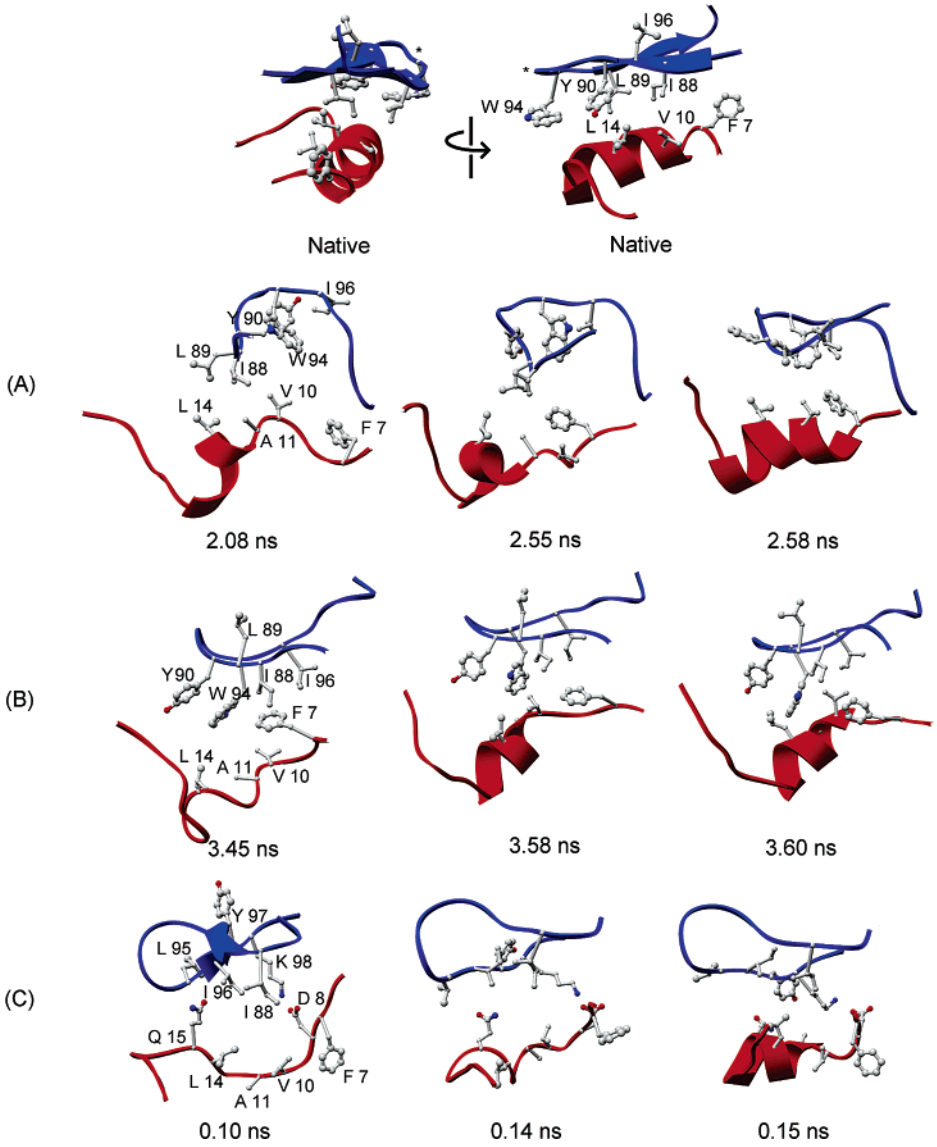

FIGURE 2: Contact-assisted helix formation in the main hydrophobic core α1/β(3−4) region of barnase. (Top) The native α1/β(3−4) fragment is shown oriented as in Figure 1 (left) and as in the other snapshots in this figure (right). Snapshots from (A) the 498 K simulation starting from the crystal structure (*31*), (B) the 498 K simulation starting from the NMR structure (*57*), and (C) the α1/β(3−4) fragment simulation.

simulation, in this case beginning from a newer crystal structure (referred to as D-3 in our previous publications), and in a fragment (discussed below). In the simulation of the full protein, α1 was completely unfolded at 3.3 ns; however, residues 9−16 had refolded by 3.6 ns (Figure 2B). At around 3.4 ns, α1 remained essentially unfolded, and contacts were formed between Phe 7 and Ile 88, across the α1 and β(3−4) interface. Over the next 100 ps, further contacts were formed at this interface, particularly between Val 10, Leu 14, and Trp 94, leading to the formation of eight residues of helical structure.

Barnase Fragment Simulations

Because of the interactions observed between α1 and β-(3−4) during the refolding of the helix in full-length protein simulations, additional simulations were performed of α1 and β(3−4) fragments, both alone and as a noncovalent complex. The fragments were slightly longer than the actual secondary structure units to reduce end effects, and the starting coordinates were extracted from the NMR solution structure.

α1 Fragment. Simulations of the α1 helix of barnase beginning from both helical and extended starting structures were performed at 498 K, the same temperature at which helix refolding was observed in simulations of the whole protein. In the unfolding simulation of the helix, the secondary structure became disrupted at 0.2 ns and was fully unstructured after 2.5 ns (Table 2). No refolding events were observed during the 25 ns trajectory. Partial folding (one turn of helix) was observed at the *C*-terminus after 24 ns in the simulation starting with the extended segment. This region of the peptide contains more hydrophobic residues than the *N*-terminus. In particular, Tyr 13 and Tyr 17 played a part in this process.

α1/β(3−4) Fragment. An α1/β(3−4) fragment (residues 5−21 and 85−100) simulation was performed for 2 ns at 498 K (*30*, *31*). This α1/β(3−4) fragment represents much of the hydrophobic core of barnase. Some helical structure was retained in α1 during this simulation; however, it was

Table 2: Average Number of Hydration Water[a] Molecules and Solvent Accessible Surface Area of Peptide in Representative Helical and Coil Regions in Fragment Simulations of Protein A Starting from Helical Conformations

	helix region[b]			coil region[b]		
	time (ns)	# waters	SASA (Å^3)	time (ns)	# waters	SASA (Å^3)
H1 448 K	0−3	129 ± 14	291 ± 87	6−7	144 ± 24	297 ± 91
498 K	7−15	122 ± 16	291 ± 85	16−19	210 ± 41	324 ± 91
H2 448 K	0−3	147 ± 11	212 ± 26	7.5−10	191 ± 19	248 ± 31
498 K	0−1	130 ± 9	221 ± 26	5−10	152 ± 20	248 ± 33
H3 448 K	0−3	128 ± 11	356 ± 25	4−6	148 ± 14	393 ± 37
498 K	0−10	138 ± 15	393 ± 37	10−18	162 ± 36	419 ± 44

[a] Water molecules that were within 4.5 Å of the nearest protein heavy atom were considered to be in the hydration layer. [b] Helical regions were defined as the time period when the helical conformations of fewer than four residues in a row were disrupted, and the coil regions were defined as the time period during which fewer than four residues in a row were in helical conformation.

in dynamic equilibrium with coil conformations. The unfolding of the helix began from the *N*-terminus, and a dynamic turn was retained at the *C*-terminus. Several factors stabilized the *C*-terminal region of α1: (A) The stable stacking of Tyr 13 and Tyr 17 was transient; the distance between the aromatic rings was less than 7 Å on average; (B) the Asp 12 side chain formed hydrogen bonds with the hydroxyl group of Thr 16; and (C) protonated His 18 capped the *C*-terminus of the helix through dynamic interactions with the carbonyl group of Gln 15. In addition to this retention of structure, there were several contact-assisted refolding events. The specific residues interacting at the interface between the secondary structural elements differed in the fragment and full-length protein simulations. However, with the exception of a salt bridge between Asp 8 and Lys 98, interactions across the α1 and β(3−4) interface were predominantly hydrophobic in nature.

The major contact-assisted refolding event occurred between 100 and 200 ps (Figure 2C). The α1 helix had essentially lost all helical structure by ∼80 ps into the simulation, with a few contacts retained across the α1/β(3−4) interface. The formation of the first turn of α1 began with the formation of a native $i \rightarrow i + 4$ backbone hydrogen bond between Leu 14 and His 18. This structure was stabilized by the capping interaction of His 18 and by the stacking of Trp 94 onto His 18. The side chain of Gln 15 played a significant role in the formation of the second turn of α1 by forming a hydrogen bond with Ala 11. The chain was then pulled in further toward the turn by the formation of an $i \rightarrow i + 3$ hydrogen bond between Ala 11 and Leu 14, which stabilized the second turn of α1. At the same time, further hydrophobic contacts were formed between α1 and β4. At ∼145 ps, the hydrophobic side chains formed a cluster between α1 and β4, and the last two turns of α1 underwent structural rearrangement involving the formation of transient $i \rightarrow i + 3$ and/or $i \rightarrow i + 4$ backbone hydrogen bonds. These hydrogen bonds flickered, and the structural rearrangements continued until the backbone atoms found their proper hydrogen bond partners at ∼150 ps. At this point, the last two turns of α1 were reformed, and Asp 12/Thr 16 interactions were restored. The stacking of Tyr 13 and Tyr 17 was not regained until approximately 200 ps, which then provided additional stabilization to the *C*-terminal region of α1.

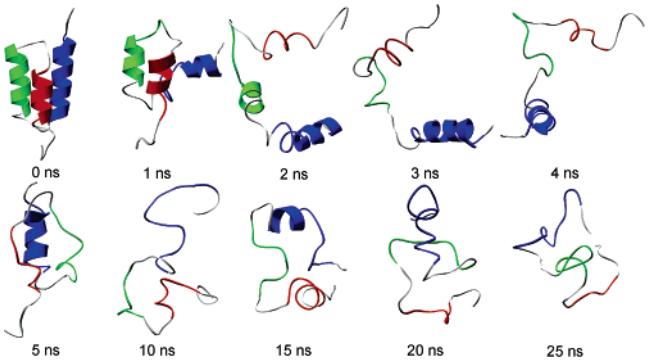

FIGURE 3: Unfolding of protein A at 498 K. Residues in helix 1 in the native structure are colored red, those in helix 2 are green, and those in helix 3 are blue. Residues in the loop regions in the native structure are gray. The wide ribbon denotes secondary structure as determined by using the Kabsch and Sander DSSP algorithm (*74*).

There is evidence from a variety of techniques that α1 and β(3−4) contain residual structure and that they are folding initiation sites (*30*, *31*). In isolation, either as fragments or in the full-length protein, these segments are only marginally stable. But, when they come together, they can stabilize one another and assist each other in refolding. Following the initiation of folding from these sites, there is further consolidation of structure along the folding reaction coordinate.

Full-Length Protein A Simulations

As with barnase, protein A fragment simulations described below were motivated by our earlier full protein simulations of different protein A domains (*32*). One simulation of the E domain at 498 K, referred to as the E2 simulation previously, has been extended here from 6 to 25 ns (Figure 3). The continuation of the simulation confirms our earlier finding that H3 is, overall, the most stable helix in multiple simulations of different protein A variants. The highly mobile nature of H1 is also obvious in this simulation. After the protein became extended and the helices separated, they sampled their local conformational space guided by their secondary structural propensities, local interactions along the helices, and interactions with their environment. After fully unfolding, the refolding of the helices occurred at various times. For example, both H1 and H2 mainly refolded from the *C*-terminus, whereas the folding of H3 was initiated from either end. H1 and H3 refolded even when they were not in contact with the rest of the protein, whereas H2 refolded only when interacting with H1 and/or H3 (Figure 4).

H2 underwent three refolding events in this simulation, at ∼5, 11, and 16 ns. The most extensive of these refolding events occurred at ∼5 ns and was triggered mainly by the hydrophobic collapse of the three segments (Figure 5A). There was a significant conformational change from 4.9 to 4.95 ns, which resulted in the formation of the first turn in the H2 segment. Before 4.9 ns, residues Phe 28, Ile 29, and Leu 32 were almost linear. By 4.91 ns, Ile 29 pointed toward the inside of the protein as it approached Phe 11 at 4.92 ns, which brought Phe 28 and Leu 32 closer to one another. At 4.93 ns, Ile 29 interacted with Val 42, Leu 43, and Phe 11, which led to a hydrophobic cluster by 4.95 ns. Although Phe 28 and Leu 32 interacted with one another, this interaction only occurred after Ile 29 had made contact with

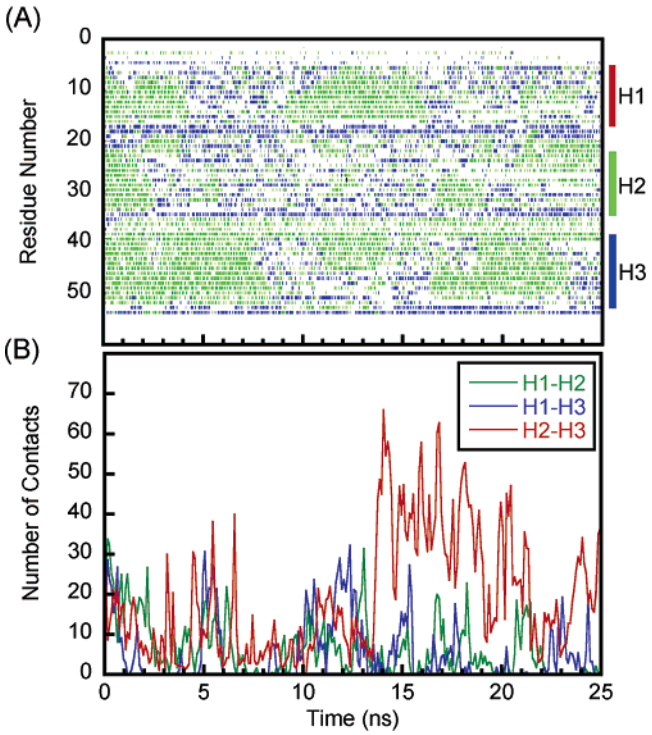

FIGURE 4: (A) Secondary structural changes in the protein A simulation at 498 K. Residues with helical conformation are indicated with a green bar, those with beta conformation with a blue bar, and all other conformations with a white bar. Conformations were determined from (ϕ,ψ) angles. (B) Variation of the number of heavy atom contacts between each pair of helical segments with time.

other residues, such as Phe 11 and Leu 43, in the center of the protein (Figure 5A). The second turn formed between 5.12 and 5.13 ns when Phe 28 and Ile 29 made further interactions with other residues in the core. These interactions pulled on the residues of the second turn, which gave them the chance to adopt more favorable conformations and find main-chain hydrogen bonding partners at 5.126 ns. From 5.124 to 5.126 ns, residues 25 and 28−31 changed conformations to helices. The last turn formed from 5.2 to 5.5 ns, when residues 24−26 converted to helical conformations via the propagation of the two existing turns, which were stabilized by hydrophobic interactions.

The folding event at 11.3 ns was similar, but less extensive. Folding began at around 11.1 ns when the residues toward the *C*-terminus of H2 formed contacts with H3 and, to a lesser extent, with H1 (Figure 5B). Residues 29−32 were the first to adopt helical conformations, followed by residues 26−28. Unlike the folding event at 5 ns, residues 24 and 25 did not adopt helical (ϕ,ψ) angles or $i \rightarrow i + 4$ hydrogen bonds. H2 also reformed partially at about 16.7 ns. In this case, H2 was in contact mainly with H3 (Figure 4). This simulation indicates that H2 and H3 have an affinity for one another and spend much time in contact, stabilizing each other in the helical state. This sequence of events was different from that of the fragment simulations in which the Phe 28/Ile 29 and Leu 32 interaction dominated the folding process.

Protein A Fragment Simulations

α-*Helical Starting Structures.* The three helices H1, H2, and H3 were simulated at three different temperatures (398, 448, and 498 K) to investigate the stability of the helical peptides when starting from their conformations in the NMR structure (*56*). To describe the unfolding and refolding events in these trajectories, we define the following events and terms: at least four successive residues had to adopt helical (ϕ,φ) angles to be considered to be in a helical conformation. If four or more neighboring residues were not helical for more than 100 ps, then that part of the helical segment was described as disrupted or unfolded. A peptide with less than three helical residues was considered to be completely unfolded.

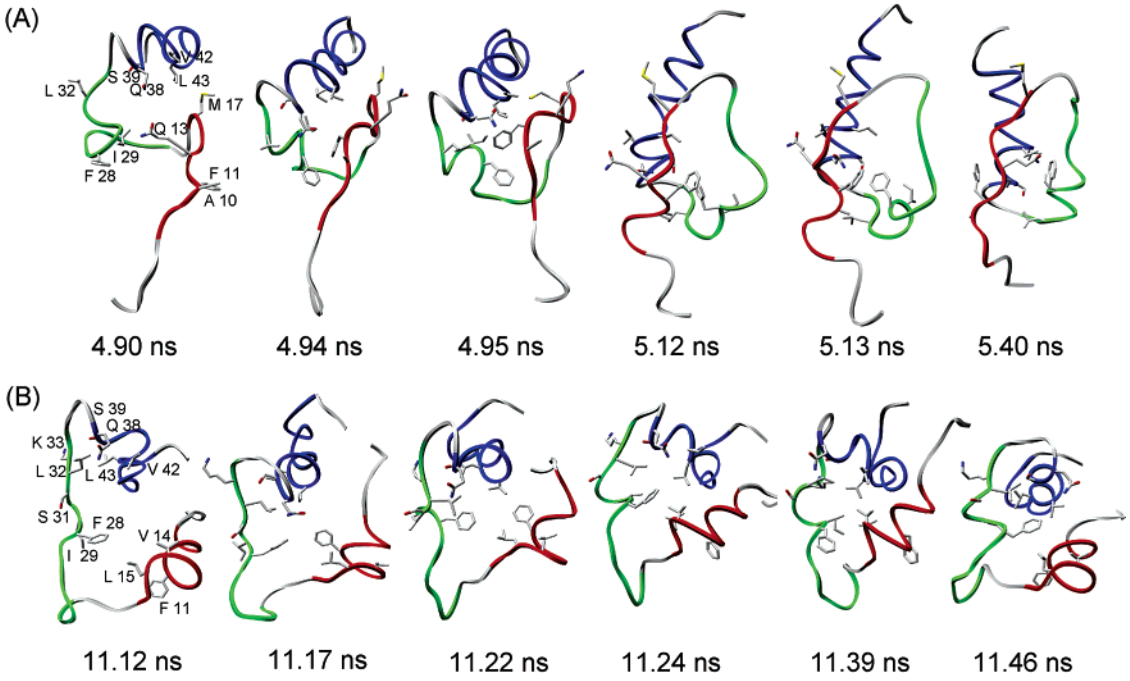

FIGURE 5: Snapshots of helix formation in the protein A simulation at 498 K. (A) Folding of helix 2 at around 5 ns. (B) Partial folding of helix 2 at around 11 ns. Residues in helix 1 in the native structure are colored red, those in helix 2 are green, and those in helix 3 are blue. Residues in the loop regions in the native structure are gray. The narrow ribbons are shown (irrespective of secondary structure) for clarity.

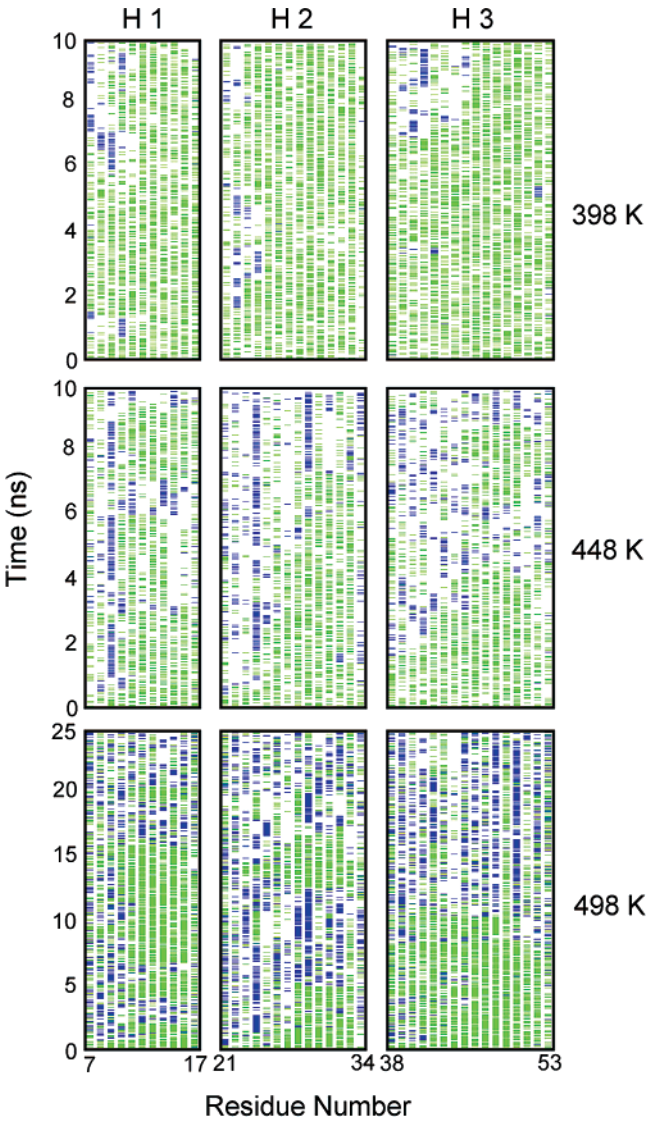

FIGURE 6: Secondary structure as a function of time for the H1, H2, and H3 fragments of protein A starting in helical conformations. Residues with helical conformation are indicated with a green bar, those with beta conformation with a blue bar, and all other conformations with a white bar. The conformations were determined from (Φ,Ψ) angles.

H1 quickly became disrupted at all temperatures (approximately 0.73, 0.6, and 0.67 ns at 398, 448, and 498 K, respectively), highlighting the instability of this fragment (Figure 6). In all cases, the unfolding of the helix began from the *N*-terminus. Interestingly, there were several folding events (i.e., reformation of helical structure) in both the 448 and 498 K trajectories. A detailed examination of the structures at the residue level reveals that the *C*-terminal hydrophobic interactions, especially side chain interactions between Phe 11 and Leu 15, dominated the folding behavior of the H1 fragment at high temperatures. That is, the helix folded from the *C*-terminus after Phe 11 and Leu 15 made contact.

H2 first became disrupted at 2.5, 0.75, and 0.2 ns at 398, 448, and 498 K, respectively, with a longer retention of H2 than H1 at low temperatures. H2 refolded after 12.5 ns at 498 K, and it persisted for 2.5 ns. This fragment basically refolded in the same manner as H1: it began from the *C*-terminus and then propagated to the *N*-terminus (Figure 6). Interactions between the side chains of Ile 29, Leu 32, and Lys 33 stabilized the first turn at the *C*-terminus at 12.63 ns, which allowed the helix to propagate toward the *N*-terminus. This sequence of events was different from that in the simulation of the whole protein, where the interaction between Phe 28 and Leu 32 occurred only after Ile 29 made tertiary contacts with H1 and/or H3.

H3 became disrupted at 3.31 and 2.23 ns at 398 and 448 K, respectively, with a longer retention of the helix than was observed for H1 and H2. The H3 helix showed some structural fluctuation at both the *N*-terminus and in the center of the sequence before 7 ns in the 498 K trajectory, but it quickly returned to the helical conformation. H3 not only was disrupted later than both H1 and H2 but also was the peptide that suffered the lowest number of disruptions before it became fully unfolded. H1 was the least stable and was disrupted more often than H2 and H3 prior to fully unfolding.

One notable feature in these trajectories is that H1 experienced more dynamic conformational changes than the other two helices. The main chain−main chain hydrogen bonds at the *C*-terminus in H1 frequently switched between α- and π-helical conformations; this phenomenon was not observed in H3 and only very transiently in H2. The behavior of some representative hydrogen bonds for each helix is shown in Figure 7. Another interesting feature of H1 was the difference in the size of the hydration layer of the helical and coil states at 498 K (122 vs 210 water molecules, respectively, Table 2), which is consistent with the increase in the solvent accessible surface area for this conversion. Indeed, the difference in the exposure of H1 in the helical and coil conformations at 498 K was larger than at 448 K (Table 2). In contrast, the differences in exposure were very similar for both H2 and H3 between the helical and coil states, regardless of the temperature, as might be expected for peptides with lower hydrophobic contents. Overall, the stability of each helical segment in the full protein simulation agrees with the fragment simulations and further confirms our previous conclusions.

Extended Strand Starting Structures. Simulations beginning from extended conformations were performed at 448 and 498 K to investigate helix folding. There were more folding events in H3 than in H1 and H2 (7, 3, and 1, respectively). The folding events happened much earlier for H3 than for H1 and H2. Combined with the findings described above, these results suggest that H3 has the greatest tendency to form a helix. Interestingly, H1 and H2 always folded from the *C*-terminus at 498 K and from the *N*-terminus at 448 K, while both the termini and the center of H3 served as initiation sites for helix formation independent of temperature. For example, in the H1 folding event at 498 K, Phe 11 and Leu 15 at the *C*-terminus approached one another at 10.2 ns (Figure 8). This interaction triggered the formation of the first helical turn and stabilized the *C*-terminus, giving the *N*-terminus time to search for interactions upon this scaffold. Main chain hydrogen bonding and side chain packing followed, allowing for propagation of the helix toward the *N*-terminus. At 448 K, on the other hand, the H1 fragment folded from the *N*-terminus. Main chain−main chain hydrogen bonding and side chain packing were the major driving forces for helix formation. The hydrophobic residues were not close enough to make a contribution to helix formation.

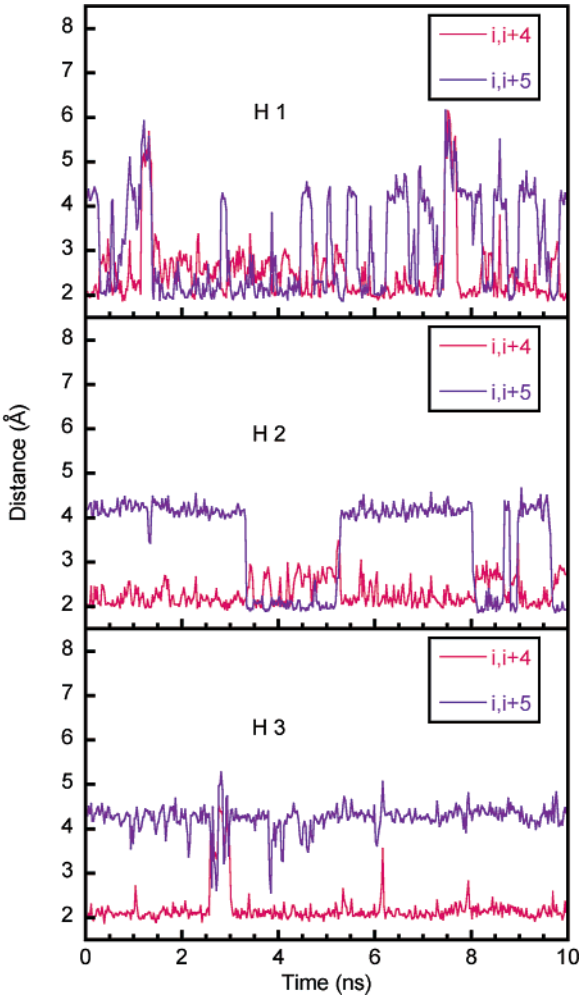

FIGURE 7: Variation of representative hydrogen bond distances with time in the 398 K simulations of the helical fragments of protein A. The $i \rightarrow i + 4$ hydrogen bonds are between residues 11 and 15, 28 and 32, and 46 and 50 in helices 1, 2, and 3, respectively. The $i \rightarrow i + 5$ hydrogen bonds extend each pair by one residue. This figure illustrates the rapid switching between α- and π-helical conformations in helix 1 compared with that in helices 2 and 3.

In the helix formation of H3 at 498 K, main chain hydrogen bonds formed from a conformation with the C═O groups of residues 46−48, all pointed in the same direction. This arrangement formed a favorable field for a hydrogen bond acceptor. Interestingly, the C═O of residue 44 formed hydrogen bonds with residues 45 and 46, first at 15.67 ns and then with residue 48 during the following 10 ps. This conformational change involved few side chain interactions. The refolding of H3 was also initiated by a hydrogen bond network that restrained the local conformation at 448 K (Figure 8). Residues Glu 45, Lys 48, and Asp 51 formed a salt bridge network at 4.3 ns. Helix formation occurred on both sides of the salt bridge and finally propagated to the termini.

As mentioned above, H2 did not fold as readily as H1 and H3. There was only one folding event in the simulations of this fragment. Helix formation was triggered by the conformational search within a very limited space because of constraints imposed by a salt bridge between Asp 23 and Lys 33. This result further supports the notion that H2 has lower helical propensity.

DISCUSSION

Mutation of Residues Important in Contact-Assisted Folding. What is the effect of the mutation of residues important in contact-assisted folding? This question is most easily addressed for barnase, where the denatured, intermediate, and transition states have been characterized, giving a picture of the residues that are structured at different stages on the protein pathway (*30*−*31*, *33*, *35*). Interactions between residues Phe 7, Val 10, and Leu 14 in α1 and residues Ile 88, Leu 89, and Trp 94 in β(3−4) were seen in the simulations to be important in contact-assisted helix formation. These residues are in regions that have been shown to be important in experimental folding studies. NMR studies of the denatured state suggest that there is residual structure in the regions of α1 and β(3−4). This residual structure is believed to play a role in initiating early folding events. Residues Val 10, Leu 14, Ile 88, and Leu 89 were mutated in a protein engineering Φ-value analysis of barnase. This study showed that all four residues are in the regions of the protein that are structured in both the intermediate and transition states, with residues Ile 88 and Leu 89, in

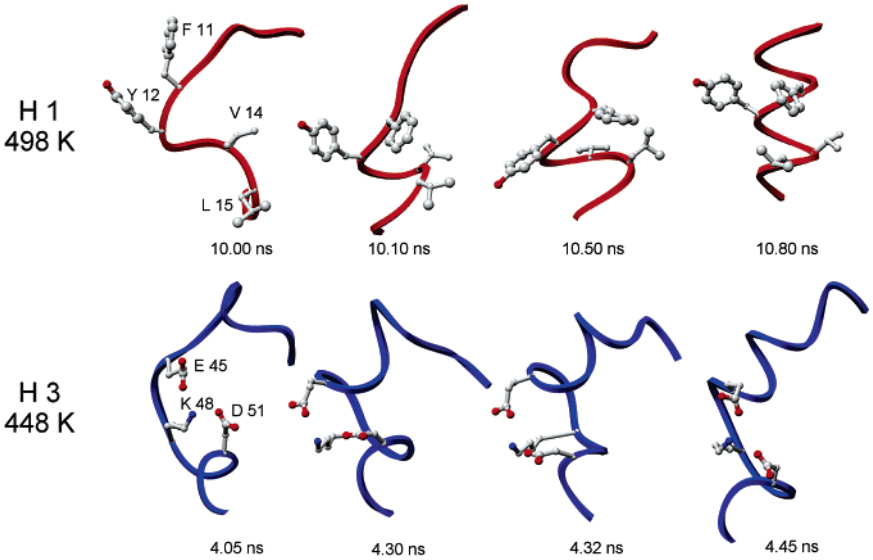

FIGURE 8: Helix formation in simulations of protein A fragments beginning from the extended structure. Residues in helix 1 in the native structure are colored red and those in helix 3 are blue. The narrow ribbons are shown (irrespective of secondary structure) for clarity.

particular, having Φ-values close to 1, or essentially native-like structure, in the transition state. The effect of the mutation of residues important in contact-assisted folding is more difficult to address for protein A. Φ-Value analysis has been carried out for a homologue of the protein studied here, the B-domain of protein A (*55*). However, protein A folds in a two-state manner; therefore, we only have a single snapshot of structure formation along the folding pathway from experiment. We have shown that residues Phe 28 and Ile 29 in H2, Phe 11 in H1, and Gln 38, Ser 39, Leu 42, and Val 43 in H3 are particularly important in contact-assisted helix formation in protein A. Many of these residues are not in contact in the native state. We postulate that non-native contacts would assist in helix formation early in folding and that side chain rearrangement would then take place later on the folding pathway. A comparison with experimental values is therefore not possible in this case.

Kinetic Stability of the Helices of Protein A. The fragment simulations performed at a variety of different temperatures demonstrate that H3 was the most stable helical fragment from protein A. Although H1 refolded easily and retained its helical conformation for some time at 498 K, it was extremely dynamic, with the main chain fluctuating between α- and π-helical conformations. π-Helical hydrogen bonding was never observed in H3 and only transiently in H2. The dynamic behavior of H1 was due to steric clashes involving its bulky side chains. As shown in Table 1, the average size of the side chains is inversely proportional to the stability of these fragments. The difference in stability between H1 and H3 suggests that large residues may destabilize the helix. This result supports the view that most residues are helix destabilizing aside from Ala (*63*, *64*). In a model peptide MD study of α- to π-helix transitions, the conformational change happened more rapidly in a peptide with larger side chains than in a peptide with smaller side chains, consistent with our results (*65*). In addition, both simulations and experiment have observed π-helix formation occurring in peptides with $i \rightarrow i + 5$ spacing of large residues (*66*−*68*).

On the basis of these arguments, it is understandable that the stability of α1 from barnase is also much lower than the H3 helix of protein A, and instead, it is similar to H1 and H2. The simulations described here show that favorable side chain interactions will catalyze helix formation as well as stabilize the helix. However, the less stable nature of H1 and H2 indicates that bulky residues may destabilize the helix when they are in unfavorable positions. Thus, unsurprisingly, the overall stability of a helix relies upon the balance of favorable side chain packing and the unfavorable steric interactions among side chains.

Mechanism of Helix Formation and the Effect of Temperature. Several different mechanisms of helix formation were observed in these simulations. It is interesting that at high temperatures, hydrophobic interactions dominated and were important for helix formation in H1 and H2 of protein A, which contain several hydrophobic residues at their *C*-termini. This effect is consistent with the temperature dependence of the hydrophobic effect (*12*, *69*). For example, the exposure of nonpolar residues was lower in the helical than in the extended conformations of H1 such that a considerable number of hydration waters were released into bulk upon folding. In contrast, hydrogen bonds dominated helix formation at lower temperatures. All of the folding events in the H1 and H2 simulations at 498 K were catalyzed by hydrophobic contacts, and those in the H1, H2, and H3 simulations at 448 K were catalyzed by hydrogen bonds or other polar interactions. Helix formation in H3 at 498 K, however, was catalyzed by hydrogen bonds, as it contains fewer hydrophobic residues than H1 and H2, especially those with $i \rightarrow i + 4$ spacing.

Helical Propensity. It is well known that β-branched or bulky residues are unfavorable in helices (*63*, *70*). Although the fragments in this study contain few β-branched residues (Table 1), the average side chain sizes are distinctive, decreasing from H1 to H3 of protein A. The average side chain size of α1 of barnase is between H1 and H2. In many of the simulations, helix formation appears to be catalyzed by hydrogen bonds/salt bridges formed between side chains or main chain and side chain atoms. In many cases, the salt bridges did not directly aid in the process of $i \rightarrow i + 4$ main chain hydrogen bond formation. Instead, they provided a scaffold for the rest of the residues to build upon by limiting conformational sampling and tethering a portion of the chain. Another common mechanism for tethering the chain was hydrophobic staples formed through interactions between nonpolar side chains. Helical turns can then propagate in both directions from these staples. Interestingly, the tether does not need to be helical with $i \rightarrow i + 4$ interactions to nucleate the helix independent of whether the helix was tethered by polar or nonpolar interactions, demonstrating the importance of nonnative interactions in folding.

Contact-Assisted Helix Formation and Its Relevance to the Mechanism of Folding. Our results show that hydrophobic contacts were very important in triggering helix formation for the segments with low helical propensity, such as H1 and H2 of protein A and α1 of barnase. A comparison of the fragment and full-length protein simulations suggests that early events in secondary structure formation rely primarily on intrinsic propensities or the intrahelical interactions. In this case, H3, which has high helical propensity and was shown to be the most stable helical segment, would form in the early stages of folding, as suggested by other studies (*32*, *48*, *50*, *51*). H2 and H3 remained near one another throughout most of the simulation after ∼14 ns in the full-length protein simulation. Because the H2−H3 motif showed higher helix content than H2 and H3 alone, as is also seen experimentally (*32*, *48*, *50*, *51*), it may serve as a scaffold for folding. Indeed, when H1 covers the H2−H3 surface in the right topology, the hydrophobic contacts and other interactions at the interface trigger the final folding of H2 to the native helical conformation of the protein. For simple protein domains composed of a few helices, knowledge of stability and helical propensity gained from coupled fragment and full-length protein simulations should be helpful in predicting folding pathways. These results may also have implications in understanding the highly cooperative nature of protein folding. On a macroscopic level, this arises because of transitions between states that are separated by an energy barrier with only the transient population of conformations between each state. The results presented here hint at one mechanism by which cooperativity may be achieved at the microscopic level. Some secondary structural elements require assistance from tertiary contacts to fold, which would lead directly to cooperativity in folding.

We have recently shown how helical propensity plays a role in the formation of a folding intermediate in the ultrafast folding of a similar 3-helix bundle, the engrailed homeodomain (*71*, *72*). For this protein, folding involves the docking of essentially preformed helices. Interestingly, a structurally homologous protein, c-Myb, with a lower helical propensity does not form a stable intermediate and instead folds via a mixed framework and a nucleation−condensation mechanism in which secondary and tertiary structure formation are more tightly coupled (*17*). Tertiary contact-assisted helix formation figures prominently during the process, and mutations increasing its helical propensity lead to the formation of a helical intermediate and a shift to folding via the framework model (*73*). Thus, the tertiary contact-assisted secondary structure formation outlined here demonstrates the importance of moving beyond the simple hierarchical models of protein folding, which in turn may provide the missing link and finally allow us to predict protein structures more reliably.

REFERENCES

1. Lindorff-Larsen, K., Rogen, P., Paci, E., Vendruscolo, M., and Dobson, C. M. (2005) Protein folding and the organization of the protein topology universe, *Trends Biochem. Sci. 30*, 13−19.
2. Onuchic, J. N., and Wolynes, P. G. (2004) Theory of protein folding, *Curr. Opin. Struct. Biol. 14*, 70−75.
3. Kubelka, J., Hofrichter, J., and Eaton, W. A. (2004) The protein folding 'speed limit', *Curr. Opin. Struct. Biol. 14*, 76−88.
4. Shea, J. E., and Brooks, C. L. (2001) From folding theories to folding proteins: A review and assessment of simulation studies of protein folding and unfolding, *Annu. Rev. Phys. Chem. 52*, 499−535.
5. Daggett, V., and Fersht, A. R. (2003) Is there a unifying mechanism for protein folding? *Trends Biochem. Sci. 28*, 18−25.
6. Radford, S. E. (2000) Protein folding: progress made and promises ahead, *Trends Biochem. Sci. 25*, 611−618.
7. Eaton, W. A., Munoz, V., Hagen, S. J., Jas, G. S., Lapidus, L. J., Henry, E. R., and Hofrichter, J. (2000) Fast kinetics and mechanisms in protein folding, *Annu. Rev. Biophys. Biomol. Struct. 29*, 327−359.
8. Kim, P. S., and Baldwin, R. L. (1982) Specific intermediates in the folding reactions of small proteins and the mechanism of protein folding, *Annu. Rev. Biochem. 51*, 459−489.
9. Ptitsyn, O. B., and Rashin, A. A. (1975) Model of myoglobin self-organization, *Biophys. Chem. 3*, 1−20.
10. Karplus, M., and Weaver, D. L. (1994) Protein-folding dynamics − the diffusion-collision model and experimental-data, *Protein Sci. 3*, 650−668.
11. Kim, P. S., and Baldwin, R. L. (1990) Intermediates in the folding reactions of small proteins, *Annu. Rev. Biochem. 59*, 631−660.
12. Kauzmann, W. (1959) Some factors in the interpretation of protein denaturation, *Adv. Protein Chem. 14*, 1−63.
13. Baldwin, R. L. (1989) How does protein folding get started, *Trends Biochem. Sci. 14*, 291−294.
14. Tanford, C. (1970) Protein denaturation, Part C, *Adv. Protein Chem. 21*, 1−95.
15. Fersht, A. R. (1997) Nucleation mechanisms in protein folding, *Curr. Opin. Struct. Biol. 7*, 3−9.
16. Daggett, V. (2002) Molecular dynamics simulations of the protein unfolding/folding reaction, *Acc. Chem. Res. 35*, 422−429.
17. Gianni, S., Guydosh, N. R., Khan, F., Caldas, T. D., Mayor, U., White, G. W. N., DeMarco, M. L., Daggett, V., and Fersht, A. R. (2003) Unifying features in protein-folding mechanisms, *Proc. Natl. Acad. Sci. U.S.A. 100*, 13286−13291.
18. Thompson, P. A., Eaton, W. A., and Hofrichter, J. (1997) Laser temperature jump study of the helix-coil kinetics of an alanine peptide interpretted as a 'kinetic zipper' model, *Biochemistry 36*, 9200−9210.
19. Williams, S., Causgrove, T. P., Gilmanshin, R., Fang, K. S., Callender, R. H., Woodruff, W. H., and Dyer, R. B. (1996) Fast Events in Protein Folding: Helix Melting and Formation in a Small Peptide, *Biochemistry 35*, 691−697.
20. Wang, T., Zhu, Y. J., Getahun, Z., Du, D. G., Huang, C. Y., DeGrado, W. F., and Gai, F. (2004) Length dependent helix-coil transition kinetics of nine alanine-based peptides, *J. Phys. Chem. B 108*, 15301−15310.
21. Huang, C.-Y., Getahun, Z., Zhu, Y., Klemke, J. W., DeGrado, W. F., and Gai, F. (2002) Helix formation via conformation diffusion search, *Proc. Natl. Acad. Sci. U.S.A. 99*, 2788−2793.
22. Daggett, V., and Levitt, M. (1992) Molecular dynamics simulations of helix denaturation, *J. Mol. Biol. 223*, 1121−1138.
23. Chowdhury, S., Zhang, W., Wu, C., Xiong, G., and Duan, Y. (2003) Breaking non-native hydrophobic clusters is the rate-limiting step in the folding of an alanine-based peptide, *Biopolymers 68*, 63−75.
24. Ferrara, P., Apostolakis, J., and Caflisch, A. (2000) Thermodynamics and kinetics of folding of two model peptides investigated by molecular dynamics simulation, *J. Phys. Chem. B 104*, 5000−5010.
25. Garcia, A. E., and Sanbonmatsu, K. Y. (2002) Alpha-helical stabilisation by side chain shielding of backbone hydrogen bonds, *Proc. Natl. Acad. Sci. U.S.A. 99*, 2782−2787.
26. Gnanakaran, S., and Garcia, A. E. (2005) Helix-coil transition of alanine peptides in water: Force field dependence on the folded and unfolded structures, *Proteins 59*, 773−782.
27. Paschek, D., Gnanakaran, S., and Garcia, A. E. (2005) Simulations of the pressure and temperature unfolding of an alpha-helical peptide, *Proc. Natl. Acad. Sci. U.S.A. 102*, 6754−6770.
28. Nymeyer, H., and Garcia, A. E. (2003) Simulation of the folding equilibrium of alpha-helical peptides: A comparison of the generalized Born approximation with explicit solvent, *Proc. Natl. Acad. Sci. U.S.A. 100*, 13934−13939.
29. Sorin, E. J., and Pande, V. S. (2005) Exploring the helix-coil transition via all-atom equibrium ensemble simulations, *Biophys. J. 88*, 2472−2493.
30. Bond, C. J., Wong, K. B., Clarke, J., Fersht, A. R., and Daggett, V. (1997) Characterization of residual structure in the thermally denatured state of barnase by simulation and experiment: Description of the folding pathway, *Proc. Natl. Acad. Sci. U.S.A. 94*, 13409−13413.
31. Wong, K. B., Clarke, J., Bond, C. J., Neira, J. L., Freund, S. M. V., Fersht, A. R., and Daggett, V. (2000) Towards a complete description of the structural and dynamic properties of the denatured state of barnase and the role of residual structure in folding, *J. Mol. Biol. 296*, 1257−1282.
32. Alonso, D. O. V., and Daggett, V. (2000) Staphylococcal protein A: Unfolding pathways, unfolded states, and differences between the B and E domains, *Proc. Natl. Acad. Sci. U.S.A. 97*, 133−138.
33. Matouschek, A., Serrano, L., and Fersht, A. R. (1992) The folding of an enzyme 4. Structure of an intermediate in the refolding of barnase analyzed by a protein engineering procedure, *J. Mol. Biol. 224*, 819−835.
34. Matouschek, A., Matthews, J. M., Johnson, C. M., and Fersht, A. R. (1994) Extrapolation to water of kinetic and equilibrium data for the unfolding of barnase in urea solutions, *Protein Eng. 7*, 1089−1095.
35. Serrano, L., Matouschek, A., and Fersht, A. R. (1992) The folding of an enzyme 3. Structure of the transition-state for unfolding of barnase analyzed by a protein engineering procedure, *J. Mol. Biol. 224*, 805−818.
36. Fersht, A. R. (1993) Protein-folding and stability - the pathway of folding of Barnase, *FEBS Lett. 325*, 5−16.
37. Arcus, V. L., Vuilleumier, S., Freund, S. M. V., Bycroft, M., and Fersht, A. R. (1995) A Comparison of the pH, urea, and temperature-denatured states of barnase by heteronuclear NMR - Implications for the initiation of protein-folding, *J. Mol. Biol. 254*, 305−321.
38. Khan, F., Chuang, J. I., Gianni, S., and Fersht, A. R. (2003) The kinetic pathway of folding of barnase, *J. Mol. Biol. 333*, 169−186.
39. Caflisch, A., and Karplus, M. (1999) Structural details of urea binding to barnase: a molecular dynamics analysis, *Struct. Fold. Des. 7*, 477−488.
40. Caflisch, A., and Karplus, M. (1995) Acid and thermal-denaturation of barnase investigated by molecular-dynamics simulations, *J. Mol. Biol. 252*, 672−708.
41. Caflisch, A., and Karplus, M. (1994) Molecular-dynamics simulation of protein denaturation - solvation of the hydrophobic cores

and secondary structure of barnase, *Proc. Natl. Acad. Sci. U.S.A. 91*, 1746−1750.
42. TiradoRives, J., Orozco, M., and Jorgensen, W. L. (1997) Molecular dynamics simulations of the unfolding of barnase in water and 8 M aqueous urea, *Biochemistry 36*, 7313−7329.
43. Li, A. J., and Daggett, V. (1998) Molecular dynamics simulation of the unfolding of barnase: Characterization of the major intermediate, *J. Mol. Biol. 275*, 677−694.
44. Daggett, V., Li, A., and Fersht, A. R. (1998) Combined molecular dynamics and phi value analysis of structure−reactivity relationships in the transition state and unfolding pathway of barnase: Structural basis of Hammond and anti-Hammond effects, *J. Am. Chem. Soc. 120*, 12740−12754.
45. Brown, N. L., Bottomley, S. P., Scawen, M. D., and Gore, M. G. (1998) A study of the interactions between an IgG-binding domain based on the B domain of staphylococcal protein A and rabbit IgC, *Mol. Biotechnol. 10*, 9−16.
46. Wright, C., Willan, K. J., Sjodahl, J., Burton, D. R., and Dwek, R. A. (1977) Interaction of protein-A and Fc-fragment of rabbit immunoglobulin-G as probed by complement-fixation and NMR-studies, *Biochem. J. 167*, 661−668.
47. Wolynes, P. G. (2004) Latest folding game results: Protein A barely frustrates computationalists, *Proc. Natl. Acad. Sci. U.S.A. 101*, 6837−6838.
48. Ghosh, A., Elber, R., and Scheraga, H. A. (2002) An atomically detailed study of the folding pathways of protein A with the stochastic difference equation, *Proc. Natl. Acad. Sci. U.S.A. 99*, 10394−10398.
49. Garcia, A. E., and Onuchic, J. N. (2003) Folding a protein in a computer: An atomic description of the folding/unfolding of protein A, *Proc. Natl. Acad. Sci. U.S.A. 100*, 13898−13903.
50. Bottomley, S. P., Popplewell, A. G., Scawen, M., Wan, T., Sutton, B. J., and Gore, M. G. (1994) The stability and unfolding of an Igg binding-protein based upon the B-domain of protein-A from *Staphylococcus-aureus* probed by tryptophan substitution and fluorescence spectroscopy, *Protein Eng. 7*, 1463−1470.
51. Bai, Y. W., Karimi, A., Dyson, H. J., and Wright, P. E. (1997) Absence of a stable intermediate on the folding pathway of protein A, *Protein Sci. 6*, 1449−1457.
52. Boczko, E. M., and Brooks, C. L. (1995) First-principles calculation of the folding free-energy of a 3-helix bundle protein, *Science 269*, 393−396.
53. Guo, Z. Y., Brooks, C. L., and Boczko, E. M. (1997) Exploring the folding free energy surface of a three-helix bundle protein, *Proc. Natl. Acad. Sci. U.S.A. 94*, 10161−10166.
54. Zhou, Y. Q., and Karplus, M. (1997) Folding thermodynamics of a model three-helix-bundle protein, *Proc. Natl. Acad. Sci. U.S.A. 94*, 14429−14432.
55. Sato, S., Religa, T. L., Daggett, V., and Fersht, A. R. (2004) Testing protein-folding simulations by experiment: B domain of protein A, *Proc. Natl. Acad. Sci. U.S.A. 101*, 6952−6956.
56. Starovasnik, M. A., Skelton, N. J., Oconnell, M. P., Kelley, R. F., Reilly, D., and Fairbrother, W. J. (1996) Solution structure of the E-domain of staphylococcal protein A, *Biochemistry 35*, 15558−15569.
57. Bycroft, M., Ludvigsen, S., Fersht, A. R., and Poulsen, F. M. (1991) Determination of the three-dimensional solution structure of barnase using nuclear magnetic resonance spectroscopy, *Biochemistry 30*, 8697−8701.
58. Levitt, M., Hirshberg, M., Sharon, R., and Daggett, V. (1995) Potential-energy function and parameters for simulations of the molecular-dynamics of proteins and nucleic-acids in solution, *Comput. Phys. Commun. 91*, 215−231.
59. Levitt, M., Hirshberg, M., Sharon, R., Laidig, K. E., and Daggett, V. (1997) Calibration and testing of a water model for simulation of the molecular dynamics of proteins and nucleic acids in solution, *J. Phys. Chem. B 101*, 5051−5061.
60. Haar, L., Gallagher, J. S., and Kell, G. S. (1984) *NBS/NRC Steam Tables: Thermodynamic and Transport Properties and Computer Programs for Vapor and Liquid States of Water in SI Units*, pp 271−276, Hemisphere Publishing Corp.: Washington, DC.
61. Kell, G. S. (1967) Precise representation of volume properties of water at one atmosphere, *J. Chem. Eng. Data 12*, 66−69.
62. Pettersen, E. F., Goddard, T. D., Huang, C. C., Couch, G. S., Greenblatt, D. M., Meng, E. C., and Ferrin, T. E. (2004) UCSF chimera - A visualization system for exploratory research and analysis, *J. Comput. Chem. 25*, 1605−1612.
63. Pace, C. N., and Scholtz, J. M. (1998) A helix propensity scale based on experimental studies of peptides and proteins, *Biophys. J. 75*, 422−427.
64. Chakrabartty, A., Kortemme, T., and Baldwin, R. L. (1994) Helix propensities of the amino-acids measured in alanine-based peptides without helix-stabilizing side-chain interactions, *Protein Sci. 3*, 843−852.
65. Lee, K. H., Benson, D. R., and Kuczera, K. (2000) Transitions from alpha to pi helix observed in molecular dynamics simulations of synthetic peptides, *Biochemistry 39*, 13737−13747.
66. Armen, R., Alonso, D. O. V., and Daggett, V. (2003) The role of alpha-, 3(10)-, and pi-helix in helix → coil transitions, *Protein Sci. 12*, 1145−1157.
67. Millhauser, G. L., Stenland, C. J., Hanson, P., Bolin, K. A., and vandeVen, F. J. M. (1997) Estimating the relative populations of 3(10)-helix and alpha-helix in Ala-rich peptides: A hydrogen exchange and high field NMR study, *J. Mol. Biol. 267*, 963−974.
68. Feig, M., MacKerell, A. D., and Brooks, C. L. (2003) Force field influence on the observation of pi-helical protein structures in molecular dynamics simulations, *J. Phys. Chem. B 107*, 2831−2836.
69. Baldwin, R. L. (1986) Temperature-dependence of the hydrophobic interaction in protein folding, *Proc. Natl. Acad. Sci. U.S.A. 83*, 8069−8072.
70. Padmanabhan, S., Marqusee, S., Ridgeway, T., Laue, T. M., and Baldwin, R. L. (1990) Relative helix-forming tendencies of nonpolar amino-acids. *Nature 344*, 268−270.
71. Mayor, U., Guydosh, N. R., Johnson, C. M., Grossmann, J. G., Sato, S., Jas, G. S., Freund, S. M. V., Alonso, D. O. V., Daggett, V., and Fersht, A. R. (2003) The complete folding pathway of a protein from nanoseconds to microseconds, *Nature 421*, 863−867.
72. Mayor, U., Johnson, C. M., Daggett, V., and Fersht, A. R. (2000) Protein folding and unfolding in microseconds to nanoseconds by experiment and simulation, *Proc. Natl. Acad. Sci. U.S.A. 97*, 13518−13522.
73. White, G. W. N., Gianni, S., Grossmann, J. G., Jemth, P., Fersht, A. R., and Daggett, V. (2005) Simulation and experiment conspire to reveal cryptic intermediates and a slide from the nucleation-condensation to framework mechanism of folding, *J. Mol. Biol. 350*, 757−775.
74. Kabsch, W., and Sander, C. (1983) Dictionary of protein secondary structure-pattern-recognition of hydrogen-bonded and geometrical features, *Biopolymers 22*, 2577−2637.

BI0517281